

Reissner-Nordström black hole lensing

Ernesto F. Eiroa^{1,*}, Gustavo E. Romero^{2,†} and Diego F. Torres^{3,‡}

¹ Instituto de Astronomía y Física del Espacio, C.C. 67, Suc. 28, 1428, Buenos Aires, Argentina

² Instituto Argentino de Radioastronomía, C.C.5, 1894 Villa Elisa, Buenos Aires, Argentina

³ Physics Department, Princeton University, NJ 08544, USA

May 28, 2018

Abstract

In this paper we study the strong gravitational lensing scenario where the lens is a Reissner-Nordström black hole. We obtain the basic equations and show that, as in the case of Schwarzschild black hole, besides the primary and secondary images, two infinite sets of relativistic images are formed. We find analytical expressions for the positions and amplifications of the relativistic images. The formalism is applied to the case of a low-mass black hole placed at the galactic halo.

PACS numbers: 04.70.-s, 04.70.Bw, 97.60.Lf

1 Introduction

The theory of General Relativity predicts the deflection of light in presence of a mass distribution. A. Einstein in 1936 [1] noted that an image due to the deflection of the light of a background star by another star can have a great magnification if the observer, the lens, and the source are highly aligned. He also pointed out that the angular separation of the images was too small to be resolved by the optical telescopes available at that time.

It was the discovering of quasars in 1963 which opened the possibility of really observing gravitational lensing effects. Quasars are very bright objects, located at cosmological distances, and have a central compact optical emitting region. When a galaxy is interposed in the line of sight to them, the resulting gravitational magnification can be large and the images are well separated in some particular cases. In 1979 the first example of gravitational lensing was discovered (the quasar QSO 0957+561 A,B).

The weak field theory of gravitational lensing, developed, among others, by Y. G. Klimov, S. Liebes, S. Refsdal, R. R. Bourassa, and R. Kantowski, has been successful in explaining the astronomical observations up to now. This theory is based on a first order expansion of the small deflection angle (for a detailed treatment see [2], and references therein).

*e-mail: eiroa@iafe.uba.ar

†e-mail: romero@irma.iar.unlp.edu.ar. Member of CONICET

‡e-mail: dtorres@princeton.edu

When the lens is a very compact object (e.g. a black hole) the weak field approximation is no longer valid. Virbhadra and Ellis recently studied the strong field situation [3]. They obtained the lens equation using an asymptotically flat background metric and analyzed the lensing by a Schwarzschild black hole in the center of the Galaxy using numerical methods. Besides the primary and secondary images, they found that there exist two infinite sets of faint relativistic images. Frittelli et al. [4] found an exact lens equation without any reference to a background metric and compared their results with those of Virbhadra and Ellis for the Schwarzschild black hole case. Bozza et al. [5] obtained analytical expressions for the positions and magnification of the relativistic images using the strong field limit approximation.

In this paper we study the lensing situation when the lens is a slowly rotating Kerr-Newman black hole. The introduction of charged bodies in the strong-field lensing theory is justified since charged black holes are thought to be final result of the catastrophic collapse of very massive ($M > 35 M_\odot$) magnetized stars. Although selective accretion from the surroundings would neutralize the charged black hole if it is located in a high-density medium, there remains the possibility that if the Kerr-Newman hole is surrounded by a co-rotating, opposite charged magnetosphere, it might not discharge so quickly. Such a configuration would present zero net charge from infinity and consequently it could survive for a significant time span ($10^3 - 10^5$ yr) if located in a low density environment [6]. Moreover, the magnetosphere would have observational effects due to particle acceleration in electrostatic polar gaps, similar to those presented by pulsars [6]. The relativistic wind created by the Kerr-Newman black hole could be responsible for detectable gamma-ray emission [7]. Hence, the study of other possible observational signatures from charged black holes presents particular interest.

In Sec. 2 of this paper we introduce the basic equations using the Reissner-Nordström's metric for the black hole and a flat background metric. The Reissner-Nordström case can be used also to study slowly rotating Kerr-Newman black holes. Highly rotating objects break the spherical symmetry introducing unnecessary complications in the lensing calculations, which do not lead to qualitatively different results. In Sec. 3 we use the strong field limit approximation to obtain analytical expressions for the positions and amplifications of the relativistic images. In Sec. 4 we calculate the positions and magnifications of the primary and secondary images using the weak field approximation. In Sec. 5 we apply the formalism to a small black hole (7 solar masses) in the galactic halo. We close with Sec. 6, where some conclusions are drawn.

2 Basic equations

In this paper we use geometrized units (speed of light in vacuum $c = 1$ and gravitational constant $G = 1$).

Black holes are characterized uniquely by M (mass), Q (charge) and S (intrinsic angular momentum) [8]. Written in the t, r, θ, φ coordinates of Boyer and Lindquist, the Kerr-Newman geometry has the form:

$$ds^2 = \frac{-\Delta}{\rho^2}(dt - a \sin^2 \theta d\varphi)^2 + \frac{\sin^2 \theta}{\rho^2}[(r^2 + a^2)d\varphi - a dt]^2 + \frac{\rho^2}{\Delta}dr^2 + \rho^2 d\theta^2, \quad (1)$$

where

$$\Delta = r^2 - 2Mr + a^2 + Q^2, \quad (2)$$

$$\rho^2 = r^2 + a^2 \cos^2 \theta, \quad (3)$$

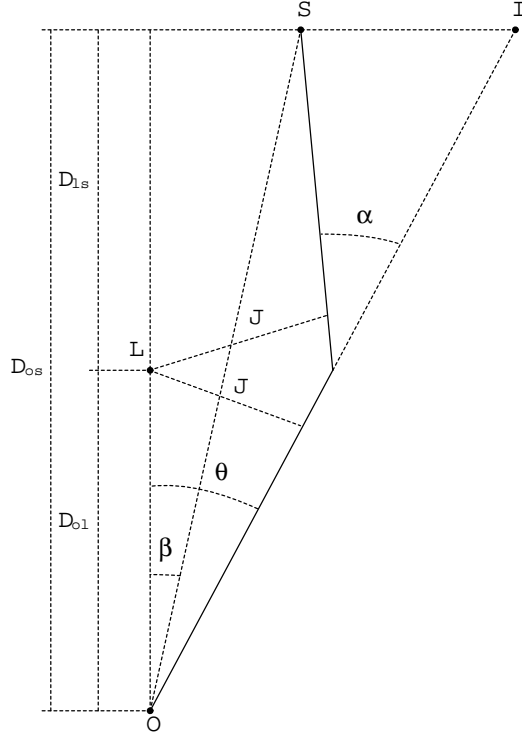


Figure 1: Lens diagram. The observer (O), the lens (L), the source (S) and the image (I) positions are shown. D_{ol} , D_{os} , D_{ls} are, respectively, the observer-lens, the observer-source and the lens-source distances. α is the deflection angle and J is the impact parameter.

$$a = \frac{S}{M}. \quad (4)$$

The Kerr-Newman geometry is axially symmetric around z axis. The horizon of events is placed at

$$r_H = r_+ = M + \sqrt{M^2 - Q^2 - a^2}. \quad (5)$$

A non-rotating black hole corresponds to an isotropic black hole with charge Q . The metric is the Reissner-Nordström's one:

$$ds^2 = - \left(1 - \frac{2M}{r} + \frac{Q^2}{r^2} \right) dt^2 + r^2 (\sin^2 \theta d\varphi^2 + d\theta^2) + \left(1 - \frac{2M}{r} + \frac{Q^2}{r^2} \right)^{-1} dr^2. \quad (6)$$

The horizon is located at

$$r_H = M + \sqrt{M^2 - Q^2}, \quad (7)$$

and the photon sphere radius is at

$$r_{ps} = \frac{3}{2}M \left(1 + \sqrt{1 - \frac{8}{9} \frac{Q^2}{M^2}} \right). \quad (8)$$

We study the lens situation shown in Fig. 1. The background space-time is considered asymptotically flat, with the observer and the source immersed in the flat space-time region, which can be

embedded, if necessary, in a Robertson-Walker expanding Universe. From Fig. 1 we see that the lens equation can be expressed [3]

$$\tan \beta = \tan \theta - \frac{D_{\text{ls}}}{D_{\text{os}}} (\tan \theta + \tan(\alpha - \theta)), \quad (9)$$

where β and θ are respectively the angular source and image positions and α is the deflection angle due to the black hole.

Following Sec. 8.5 of [9], we have that the deflection angle for a light ray is

$$\alpha(r_0) = 2 \int_{r_0}^{\infty} \frac{dr}{r \sqrt{\left(\frac{r}{r_0}\right)^2 \left(1 - \frac{2M}{r_0} + \frac{Q^2}{r_0^2}\right) - \left(1 - \frac{2M}{r} + \frac{Q^2}{r^2}\right)}} - \pi, \quad (10)$$

where r_0 is the closest distance of approach. The impact parameter is

$$J(r_0) = r_0 \left(1 - \frac{2M}{r_0} + \frac{Q^2}{r_0^2}\right)^{-\frac{1}{2}}. \quad (11)$$

From the lens diagram (Fig. 1) we see that

$$J(r_0) = D_{\text{ol}} \sin \theta. \quad (12)$$

Defining the distances and the charge in terms of the Schwarzschild radius ($2M$):

$$\begin{aligned} x &= \frac{r}{2M}, & x_0 &= \frac{r_0}{2M}, & b &= \frac{J}{2M}, \\ d_{\text{ol}} &= \frac{D_{\text{ol}}}{2M}, & d_{\text{os}} &= \frac{D_{\text{os}}}{2M}, & d_{\text{ls}} &= \frac{D_{\text{ls}}}{2M}, \\ q &= \frac{Q}{2M}, \end{aligned}$$

we have that

$$\alpha(x_0) = 2 \int_{x_0}^{\infty} \frac{dx}{x \sqrt{\left(\frac{x}{x_0}\right)^2 \left(1 - \frac{1}{x_0} + \frac{q^2}{x_0^2}\right) - \left(1 - \frac{1}{x} + \frac{q^2}{x^2}\right)}} - \pi, \quad (13)$$

$$b(x_0) = x_0 \left(1 - \frac{1}{x_0} + \frac{q^2}{x_0^2}\right)^{-\frac{1}{2}} = d_{\text{ol}} \sin \theta, \quad (14)$$

$$x_{\text{H}} = \frac{1}{2} + \sqrt{\frac{1}{4} - q^2}, \quad (15)$$

$$x_{\text{ps}} = \frac{3}{4} \left(1 + \sqrt{1 - \frac{32}{9}q^2}\right). \quad (16)$$

The deflection angle α for a light ray passing at the right of the black hole is plotted as a function of the closest approach distance x_0 in Fig. 2. We see that when x_0 takes values near x_{ps} the angle of

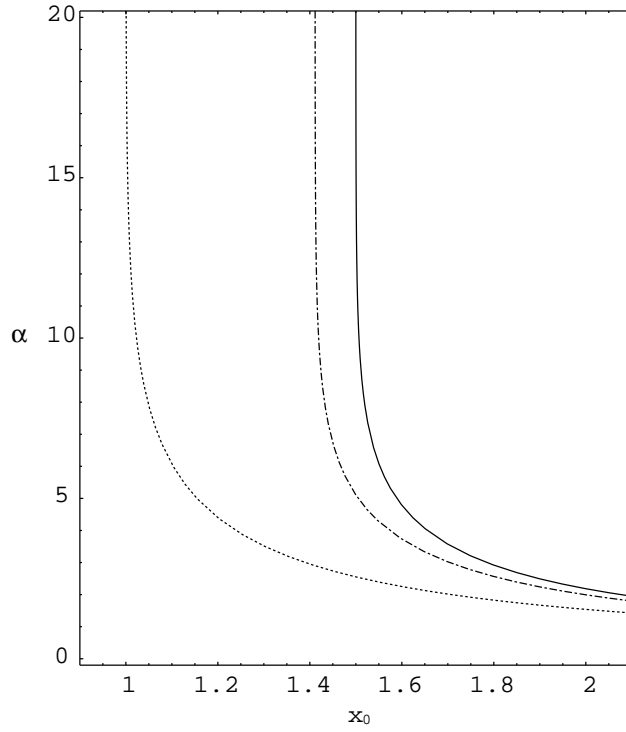


Figure 2: Deflection angle α (in radians) plotted as a function of the closest approach distance x_0 . The solid line corresponds to $Q = 0$, the dash-dot line to $|Q| = 0.5M$ and the dot line to $|Q| = M$. In each curve the vertical asymptote is placed at $x_0 = x_{ps}$.

deflection α is greater than 2π , so the light ray can take several turns around the black hole before reaching the observer. In this way, besides the primary and secondary images (with $|\alpha| < 2\pi$), we have two infinite sets of relativistic images, one produced by clockwise winding around the black hole ($\alpha > 0$) and the other by counter-clockwise winding ($\alpha < 0$). These images are located, respectively, at the same side and at the opposite side of the source. This is qualitatively shown in Fig. 3.

For a given source position β , we must solve Eq. (9) with Eqs. (13) and (14) to obtain the positions of the images. The transcendental equation (9) is hard to solve even numerically.

The magnification for a circular symmetric lens is given by

$$\mu = \left| \frac{\sin \beta \frac{d\beta}{d\theta}}{\sin \theta \frac{d\theta}{d\theta}} \right|^{-1}. \quad (17)$$

Differentiating both sides of Eq. (9) and with some algebra, we have

$$\frac{d\beta}{d\theta} = \left(\frac{\cos \beta}{\cos \theta} \right)^2 \left\{ 1 - \frac{d_{ls}}{d_{os}} \left[1 + \left(\frac{\cos \theta}{\cos(\alpha - \theta)} \right)^2 \left(\frac{d\alpha}{d\theta} - 1 \right) \right] \right\}, \quad (18)$$

where

$$\frac{d\alpha}{d\theta} = \frac{d\alpha}{dx_0} \frac{dx_0}{d\theta}, \quad (19)$$

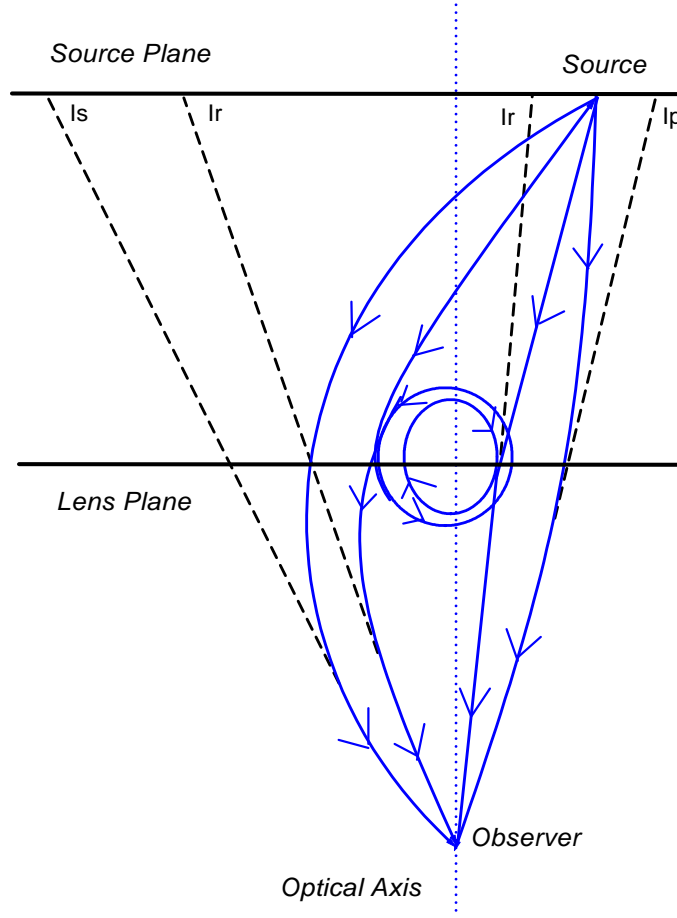


Figure 3: The primary(I_p) and secondary (I_s) images are formed when the deflection angle is (in modulus) smaller than 2π . The relativistic images (I_R) are obtained when the deflection angle is (in modulus) greater than 2π (the first with clockwise winding and the first with counter-clockwise winding are shown).

with

$$\frac{d\alpha}{dx_0} = \int_{x_0}^{\infty} \frac{-x^4(x_0 - 2q^2) + x_0^4(x - 2q^2)}{x_0^5 x^3 \left[\left(\frac{x}{x_0} \right)^2 \left(1 - \frac{1}{x_0} + \frac{q^2}{x_0^2} \right) - \left(1 - \frac{1}{x} + \frac{q^2}{x^2} \right) \right]^{\frac{3}{2}}} dx, \quad (20)$$

obtained by differentiating Eq. (13) and

$$\frac{dx_0}{d\theta} = \frac{x_0^2 \left(1 - \frac{1}{x_0} + \frac{q^2}{x_0^2} \right)^{\frac{3}{2}} \sqrt{1 - \left(\frac{x_0}{d_{ol}} \right)^2 \left(1 - \frac{1}{x_0} + \frac{q^2}{x_0^2} \right)^{-1}}}{\frac{1}{2d_{ol}} (2x_0^2 - 3x_0 + 2q^2)}, \quad (21)$$

obtained by differentiating both sides of Eq. (14) and doing some extra algebraic tricks.

3 Strong field limit

In this section we shall do some approximations. The first one is that when the source and the lens are almost aligned we can replace $\tan \theta$ by θ and $\tan \beta$ by β . For the relativistic images with clockwise winding of the rays around the black hole, we can write $\alpha = 2n\pi + \Delta\alpha_n$ with n integer and $0 < \Delta\alpha_n \ll 1$, so that $\tan(\alpha - \theta)$ can be approximated by $\Delta\alpha_n - \theta$. As in the case of Schwarzschild black hole lensing, if a ray of light emitted by the source S is going to reach the observer after turning around the black hole, α must be very close to a multiple of 2π .

Then the lens equation takes the form [5]:

$$\beta = \theta - \frac{D_{ls}}{D_{os}} \Delta\alpha_n = \theta - \frac{d_{ls}}{d_{os}} \Delta\alpha_n, \quad (22)$$

and the impact parameter is

$$b \approx \frac{D_{ol}}{2M} \theta = d_{ol} \theta. \quad (23)$$

The relativistic images are formed when the light rays pass very close to the photon sphere. So it is convenient to write the closest approach distance x_0 as

$$x_0 = x_{ps} + \varepsilon, \quad (24)$$

where $0 \leq \varepsilon \ll 1$. Bozza et al [5] have shown for the Schwarzschild black hole that the deflection angle can be approximated by:

$$\alpha = -2 \ln \left(\frac{2 + \sqrt{3}}{18} \varepsilon \right) - \pi. \quad (25)$$

From Fig. 2 we see that the curves representing the deflection angle have similar form for the different values of Q . Therefore, we shall also look for a similar approximation

$$\alpha = -A \ln(B\varepsilon) - \pi, \quad (26)$$

where A and B are to-be-defined positive numbers which will depend only on $q = Q/2M$.

A and B are chosen to satisfy

$$\lim_{x_0 \rightarrow x_{ps}} (\alpha_{\text{exact}} - \alpha_{\text{approx.}}) = 0, \quad (27)$$

with α_{exact} given by Eq. (13)¹ and $\alpha_{\text{approx.}}$ is given by Eq. (26). Eq. (27) can be written in the form

$$\lim_{x_0 \rightarrow x_{ps}} \left[\alpha_{\text{approx.}} \left(\frac{\alpha_{\text{exact}}}{\alpha_{\text{approx.}}} - 1 \right) \right] = 0. \quad (28)$$

A necessary (but not sufficient) condition for this limit is:

$$\lim_{x_0 \rightarrow x_{ps}} \frac{\alpha_{\text{exact}}}{\alpha_{\text{approx.}}} = 1. \quad (29)$$

As $\alpha \rightarrow \infty$ when $x_0 \rightarrow x_{ps}$, using the L'Hospital's rule in the limit of Eq. (29), it is easy to find A :

$$A = \lim_{x_0 \rightarrow x_{ps}} \left[-(x_0 - x_{ps}) \frac{d\alpha_{\text{exact}}}{dx_0} \right], \quad (30)$$

¹The integral of Eq. (13) can be calculated in terms of elliptic integrals and it is done in the Appendix, Eq. (73).

with $\frac{d\alpha_{\text{exact}}}{dx_0}$ given by Eq. (20)².

To obtain B , we replace Eq.(26) in Eq. (27):

$$\lim_{x_0 \rightarrow x_{\text{ps}}} [\alpha_{\text{exact}} + A \ln B(x_0 - x_{\text{ps}}) + \pi] = 0, \quad (31)$$

which, using properties of logarithms can be expressed as

$$\lim_{x_0 \rightarrow x_{\text{ps}}} A \ln \left[B(x_0 - x_{\text{ps}}) \exp \left(\frac{\alpha_{\text{exact}} + \pi}{A} \right) \right] = 0, \quad (32)$$

so

$$\lim_{x_0 \rightarrow x_{\text{ps}}} B(x_0 - x_{\text{ps}}) \exp \left(\frac{\alpha_{\text{exact}} + \pi}{A} \right) = 1, \quad (33)$$

then

$$B = \lim_{x_0 \rightarrow x_{\text{ps}}} \frac{\exp \left[\frac{-(\alpha_{\text{exact}} + \pi)}{A} \right]}{(x_0 - x_{\text{ps}})}. \quad (34)$$

A and B are given in Table 1 for some values of Q .

Table 1: Numerical values for the coefficients A and B . See text for explanation.

| $ Q $ | 0 | $0.1M$ | $0.25M$ | $0.5M$ | $0.75M$ | $1M$ |
|-------|----------|----------|---------|----------|----------|----------|
| A | 2.00000 | 2.00224 | 2.01444 | 2.06586 | 2.19737 | 2.82843 |
| B | 0.207338 | 0.207979 | 0.21147 | 0.225997 | 0.262085 | 0.426782 |

The ratio $\alpha_{\text{exact}}/\alpha_{\text{approx.}}$ is plotted in Fig. 4 for $0 \leq \varepsilon \leq 0.05$. The error using $\alpha_{\text{approx.}}$ is very small, less than 1.5 percent for $|Q| \leq 0.5M$ and less than 2 percent for $0.5M \leq |Q| \leq M$.

The impact parameter given by Eq. (14) can be approximated, using a second order Taylor expansion in ε , by

$$b = C + D\varepsilon^2, \quad (35)$$

with

$$C = \frac{(3 + \sqrt{9 - 32q^2})^2}{4\sqrt{6 - 16q^2 + 2\sqrt{9 - 32q^2}}}, \quad (36)$$

and

$$D = \frac{72 - 256q^2}{(9 - 32q^2 + \sqrt{9 - 32q^2})\sqrt{6 - 16q^2 + 2\sqrt{9 - 32q^2}}}, \quad (37)$$

where we have made use of Eqs. (16, 24). Inverting the Eq. (35) to obtain ε

$$\varepsilon = \sqrt{\frac{b - C}{D}}, \quad (38)$$

replacing Eqs. (23) and (38) in Eq. (26) we have

$$\alpha \approx -A \ln \left(B \sqrt{\frac{d_{\text{ol}}\theta - C}{D}} \right) - \pi. \quad (39)$$

²Or, in terms of elliptic integrals, by Eq. (79) of the Appendix.

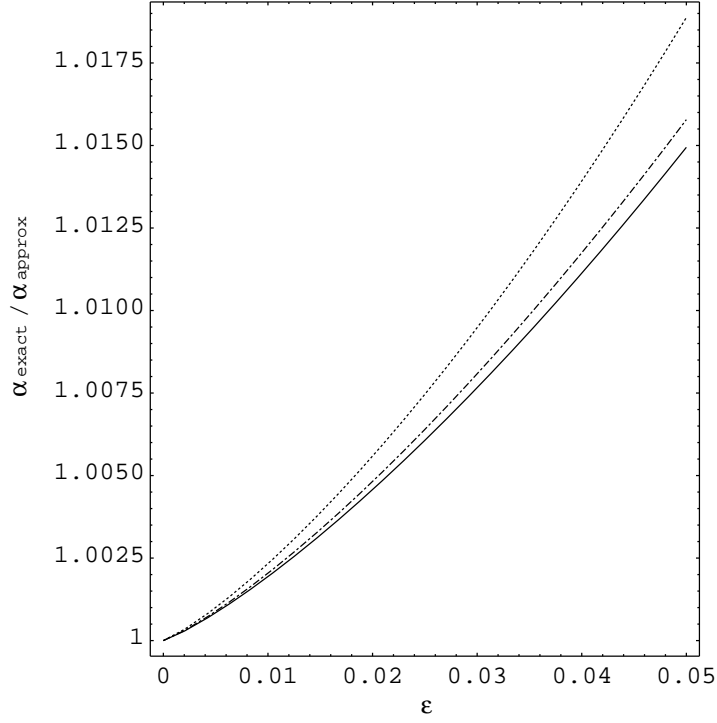


Figure 4: The ratio $\alpha_{\text{exact}}/\alpha_{\text{approx}}$, plotted as a function of $\varepsilon = x_0 - x_{\text{ps}}$. The solid line corresponds to $Q = 0$, the dash-dot line to $|Q| = 0.5M$ and the dot line to $|Q| = M$.

The position of the n -th relativistic image can be approximated by a first order Taylor expansion around $\alpha = 2n\pi$

$$\theta_n \approx \theta_n^0 - \rho_n \Delta\alpha_n, \quad (40)$$

with

$$\theta_n^0 = \theta(\alpha = 2n\pi), \quad (41)$$

and

$$\rho_n = - \left. \frac{d\theta}{d\alpha} \right|_{\alpha=2n\pi}. \quad (42)$$

Inverting Eq. (39) we have that

$$\theta = \frac{1}{d_{\text{ol}}} \left\{ \frac{D}{B^2} \exp \left[\frac{-2}{A} (\alpha + \pi) \right] + C \right\}, \quad (43)$$

then

$$\theta_n^0 = \frac{1}{d_{\text{ol}}} \left\{ \frac{D}{B^2} \exp \left[\frac{-2}{A} (2n+1)\pi \right] + C \right\}, \quad (44)$$

and

$$\rho_n = \frac{2D}{d_{\text{ol}}AB^2} \exp \left[\frac{-2}{A} (2n+1)\pi \right]. \quad (45)$$

From Eq. (40)

$$\Delta\alpha_n \approx \frac{\theta_n - \theta_n^0}{-\rho_n}, \quad (46)$$

replacing it in the lens equation, Eq. (22):

$$\begin{aligned}\beta &= \theta_n + \frac{d_{ls}}{d_{os}} \frac{\theta_n - \theta_n^0}{\rho_n} \\ &= \left(1 + \frac{d_{ls}}{d_{os}\rho_n}\right) \theta_n + \frac{d_{ls}}{d_{os}\rho_n} \theta_n^0.\end{aligned}\quad (47)$$

Using that $\rho_n \propto \frac{1}{d_{ol}}$, then $\frac{d_{ls}}{d_{os}\rho_n} \propto \frac{d_{ls}d_{ol}}{d_{os}} \gg 1$, we can neglect the 1 inside the parentheses to obtain the approximate positions of the relativistic images:

$$\theta_n = \theta_n^0 + \frac{d_{os}\rho_n}{d_{ls}} \beta. \quad (48)$$

Note that the second term in the last equation is a small correction on θ_n^0 . When the source and the lens are aligned, $\beta = 0$ and we obtain the relativistic Einstein rings with angular radius $\theta_n^E = \theta_n^0$.

The amplification of the n-th image is given by

$$\mu_n \approx \left| \frac{\beta}{\theta_n} \frac{d\beta}{d\theta_n} \right|^{-1}, \quad (49)$$

which, using Eq. (48), gives

$$\mu_n = \left| \left(\theta_n^0 + \frac{d_{os}\rho_n}{d_{ls}} \beta \right) \frac{d_{os}\rho_n}{\beta d_{ls}} \right|, \quad (50)$$

neglecting the term with $\left(\frac{d_{os}\rho_n}{d_{ls}}\right)^2$ we have

$$\mu_n \approx \frac{1}{|\beta|} \frac{d_{os}}{d_{ls}} \theta_n^0 \rho_n. \quad (51)$$

We see that $\mu_n \propto \frac{d_{os}}{\beta d_{ls} d_{ol}^2}$, so the amplification of the relativistic images is very small unless the observer, the lens and the source are highly aligned.

With a similar treatment for the images formed with counter-clockwise winding of light rays around the black hole, the positions of the relativistic images are

$$\theta_n = -\theta_n^0 + \frac{d_{os}\rho_n}{d_{ls}} \beta, \quad (52)$$

and the amplifications are given again by Eq. (51), but with opposite parity.

To obtain the total magnification of the relativistic images, we must take into account both sets of relativistic images, and sum

$$\mu_R = 2 \sum_{n=1}^{\infty} \mu_n = \frac{2}{|\beta|} \frac{d_{os}}{d_{ls}} \sum_{n=1}^{\infty} \theta_n^0 \rho_n, \quad (53)$$

which, using that the sum of a geometrical series is $\sum_{n=1}^{\infty} a^n = \frac{a}{1-a}$ for $|a| < 1$, gives

$$\mu_R \approx \frac{1}{|\beta|} \frac{d_{os}}{d_{ls} d_{ol}^2} \frac{4D}{AB^2} \left(\frac{D}{B^2} \frac{e^{-12\pi/A}}{1 - e^{-8\pi/A}} + C \frac{e^{-6\pi/A}}{1 - e^{-4\pi/A}} \right). \quad (54)$$

4 Primary and secondary images

We saw in the last section that relativistic images have a very small amplification unless the alignment is high. Now we shall obtain the positions and amplifications for the primary and secondary images in the approximation of very small source angle (β).

Very small β implies, from the lens equation, that α is very small too for the primary (P) and secondary images (S), so we can use the weak field approximation to obtain the positions and amplifications. The first step is to calculate the deflection angle α . Expanding the integrand of Eq. (13) and doing the integration we have that

$$\alpha = \frac{2}{x_0} + \left[\left(\frac{15}{16}\pi - 1 \right) - \frac{3}{4}\pi q^2 \right] \frac{1}{x_0^2} + \mathcal{O}\left(\frac{1}{x_0^3}\right). \quad (55)$$

The charge only introduces a small correction in the second order term of the deflection angle. As usual in the weak field approximation, we shall use a first order expansion, taking $\alpha \approx 2/x_0$ and $b \approx x_0 \approx d_{ol}\theta$. Introducing α in the lens equation and inverting it to obtain the positions of the images, we have:

$$\theta_p = \frac{1}{2} \left(\beta + \sqrt{\beta^2 + 4\theta_E^2} \right) \approx \theta_E + \frac{1}{2}\beta, \quad (56)$$

$$\theta_s = \frac{1}{2} \left(\beta - \sqrt{\beta^2 + 4\theta_E^2} \right) \approx -\theta_E + \frac{1}{2}\beta, \quad (57)$$

where $\theta_E = \sqrt{\frac{2d_{ls}}{d_{os}d_{ol}}}$ is the Einstein ring angular radius. Using Eq. (17), the amplifications are given by:

$$\mu_p = \frac{\left(\frac{\beta}{\theta_E}\right)^2 + 2}{2\left|\frac{\beta}{\theta_E}\right|\sqrt{\left(\frac{\beta}{\theta_E}\right)^2 + 4}} + \frac{1}{2} \approx \frac{\theta_E}{2|\beta|}, \quad (58)$$

$$\mu_s = \frac{\left(\frac{\beta}{\theta_E}\right)^2 + 2}{2\left|\frac{\beta}{\theta_E}\right|\sqrt{\left(\frac{\beta}{\theta_E}\right)^2 + 4}} - \frac{1}{2} \approx \frac{\theta_E}{2|\beta|}. \quad (59)$$

So, the total amplification μ_{wf} of the weak field images is

$$\mu_{wf} = \mu_p + \mu_s \approx \frac{\theta_E}{|\beta|} = \frac{1}{|\beta|} \sqrt{\frac{2d_{ls}}{d_{os}d_{ol}}}. \quad (60)$$

Dividing Eq. (54) by (60) we have that

$$\frac{\mu_R}{\mu_{wf}} = \left(\frac{d_{os}}{d_{ls}d_{ol}} \right)^{\frac{3}{2}} f(q), \quad (61)$$

where

$$f(q) = \frac{4D}{\sqrt{2}AB^2} \left(\frac{D}{B^2} \frac{e^{-12\pi/A}}{1 - e^{-8\pi/A}} + C \frac{e^{-6\pi/A}}{1 - e^{-4\pi/A}} \right). \quad (62)$$

$f(q)$ takes values between 1×10^{-2} and 3×10^{-2} , for $|q| \in [0, 0.5]$, so the relativistic images are much less amplified than the weak field images. To give an example, the prefactor multiplying $f(q)$ is $(\mathcal{D}/2M)^{-3/2}$, if the lens is halfway between the observer and the source, $\mathcal{D} \approx D_{os}/4$ which, unless the black hole is very massive and or near the Earth makes the amplification extremely small.

5 An example: black hole in the galactic halo

In this section we consider as a lens a black hole with mass $M = 7M_\odot$, negligible angular momentum ($S \approx 0$) and charge Q placed at the galactic halo ($D_{\text{ol}} = 4\text{kpc}$) [10]. The source is a star with radius $R_s = R_\odot$ located in the galactic bulge ($D_{\text{os}} = 8\text{kpc}$). This provides a model for lensing by black hole candidates similar to the case discussed in Ref. [7] and is only intended to give some feeling of the numerical values implied in the strong field lensing of charged compact objects.

The positions and magnifications of the relativistic images for a point source are given, respectively, by Eqs. (48, 52) and (51). The weak field images are formed near the Einstein angular radius $\theta_E \approx 2.669\text{mas}$ (milliarc second). The relativistic images have angular radius of the order of the relativistic Einstein rings, the outer one is θ_1^E and the others approach to θ_∞^E . In Table 2 the angular positions of the horizon, the photon sphere, the outer Einstein ring and the limiting value of the Einstein rings are given for different values of Q .

Table 2: Angular positions of the horizon, the photon sphere, the outer Einstein ring (θ_1^E) and the limiting value of the Einstein rings (θ_∞^E) for different values of Q .

| $ Q $ | 0 | $0.1M$ | $0.5M$ | M |
|-------------------------|------------------------|------------------------|------------------------|------------------------|
| θ_H (mas) | 3.455×10^{-8} | 3.447×10^{-8} | 3.224×10^{-8} | 1.727×10^{-8} |
| θ_{ps} (mas) | 5.181×10^{-8} | 5.171×10^{-8} | 4.876×10^{-8} | 3.455×10^{-8} |
| θ_1^E (mas) | 8.987×10^{-8} | 8.973×10^{-8} | 8.595×10^{-8} | 6.957×10^{-8} |
| θ_∞^E (mas) | 8.977×10^{-8} | 8.960×10^{-8} | 8.581×10^{-8} | 6.910×10^{-8} |

The source is extended, so we have to integrate over its luminosity profile to obtain the magnification:

$$\mu = \frac{\iint_S \mathcal{I} \mu_p dS}{\iint_S \mathcal{I} dS} \quad (63)$$

where \mathcal{I} is the surface intensity distribution of the source and μ_p is the magnification corresponding to each point of the source. We take the source as uniform, so

$$\mu = \frac{\iint_S \mu_p dS}{\iint_S dS}. \quad (64)$$

For both the relativistic and the weak field cases, the amplifications for a point source are proportional to $1/\beta$:

$$\mu \propto I = \frac{\iint_S \frac{1}{\beta} dS}{\iint_S dS}. \quad (65)$$

To obtain I we use polar coordinates (R, φ) in the source plane, with $R = 0$ in the optical axis, and take the source as a disk $D(R_C, R_S)$ of radius R_S centered in R_C . Then

$$I = \frac{\iint_{D(R_C, R_S)} \frac{1}{\beta} R dR d\varphi}{\pi R_S^2}, \quad (66)$$

and, using that $\beta = R/D_{\text{os}}$ is the angular position of each point of the source, we have

$$I = \frac{\iint_{D(\beta_C, \beta_S)} \frac{1}{\beta} \beta d\beta d\varphi}{\pi \beta_S^2} = \frac{\iint_{D(\beta_C, \beta_S)} d\beta d\varphi}{\pi \beta_S^2}. \quad (67)$$

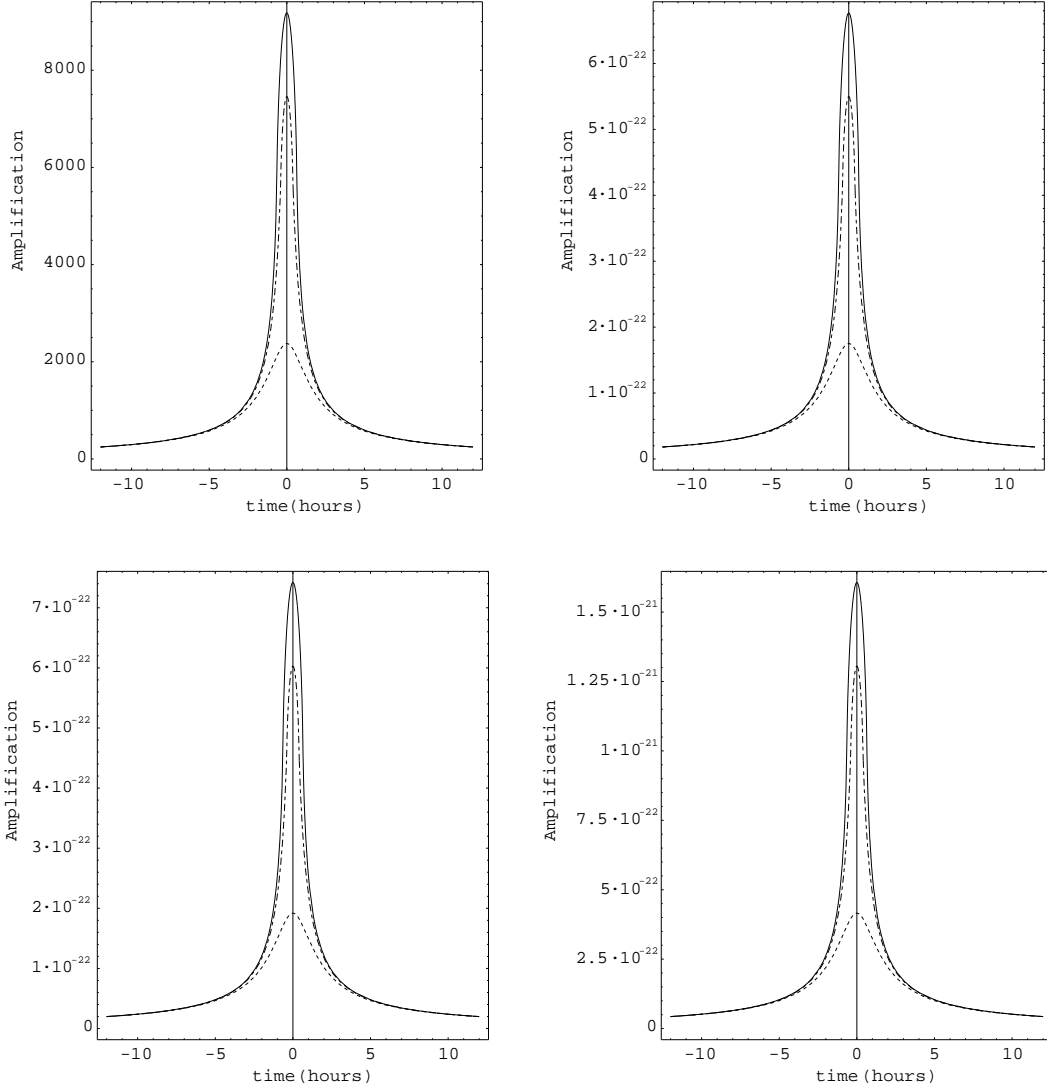


Figure 5: Light curves for a lensing event by a black hole with mass $M = 7M_\odot$ and charge Q placed at the galactic halo. The source is a star of radius $R_s = R_\odot$ placed at the galactic bulge. Upper panel, left: total amplification of the primary and secondary images. Upper panel, right: $Q = 0$, total amplification of the relativistic images. Lower panel, left: $|Q| = 0.5M$, total amplification of the relativistic images. Lower panel, right: $|Q| = M$, total amplification of the relativistic images. In all plots, the solid line corresponds to $\beta_0 = 0$, the dash-dot line to $\beta_0 = 0.8\beta_s$ and the dot line to $\beta_0 = 2\beta_s$.

where $D(\beta_c, \beta_s)$ is the disk with angular radius $\beta_s = 5.8 \times 10^{-4}$ mas centered in β_c . The last integral can be calculated in terms of elliptic functions [5]:

$$\begin{aligned}
 I = & \frac{2\text{Sign}[\beta_s - \beta_c]}{\pi\beta_s^2} \left[(\beta_s - \beta_c) E\left(\frac{\pi}{2}, -\frac{4\beta_s\beta_c}{(\beta_s - \beta_c)^2}\right) + \right. \\
 & \left. + (\beta_s + \beta_c) F\left(\frac{\pi}{2}, -\frac{4\beta_s\beta_c}{(\beta_s - \beta_c)^2}\right) \right], \tag{68}
 \end{aligned}$$

where

$$F(\phi_0, \lambda) = \int_0^{\phi_0} (1 - \lambda \sin^2 \phi)^{-\frac{1}{2}} d\phi, \quad (69)$$

$$E(\phi_0, \lambda) = \int_0^{\phi_0} (1 - \lambda \sin^2 \phi)^{\frac{1}{2}} d\phi, \quad (70)$$

are elliptic integrals of the first and second kind respectively, with the arguments ϕ_0 and λ .

In Fig. 5 the light curves for a transit event are shown. The relative velocity between the lens and the source is $v = 300 \text{ km/s}$. The angular position of the center of the source is given by $\beta_c = \sqrt{\beta_0^2 + \left(\frac{vt}{D_{\text{os}}}\right)^2}$, where β_0 is the minimum angular position of the center of the source corresponding to $t = 0$. We see that the transit event takes only a few hours, with great amplification for the weak field images and, as expected, a negligible magnification for the relativistic images. However, it is interesting to remark that with the presence of charge the amplification of the relativistic images increases respect to the Schwarzschild case. For a charge $|Q| = 0.5M$ we have about 10 % more amplification than in a similar black hole with no charge. In the case $|Q| = 1M$ the total amplification of the relativistic images is about 140 % stronger than the corresponding value for a Schwarzschild black hole of the same mass.

6 Conclusions

In this paper we developed the formalism for charged black hole lensing. We find the positions and magnifications of the relativistic images within the strong field limit. The relativistic images are more prominent when there is a close alignment between the observer, the lens, and the source. They are, though, very faint, even with complete alignment, but much stronger than in the case of Schwarzschild black holes for large charges. The angular separation of the relativistic images is beyond the angular resolution of current optical technologies. For local black holes (e.g. in the Gould Belt, a star forming region at 600 pc), however, if radio or X-ray background sources can be used, the angular separations of μas could be resolved with space techniques.

The NASA Constellation-X [11] mission, to be launched in 2008, is optimized to study the iron $K\alpha$ line features and will determine the black hole mass and spin for a large number of systems. Still, Constellation-X will provide an indirect measure of the properties of the region within a few event horizon radii. NASA-planned MAXIM mission [12], a $\mu\text{-arcsec}$ X-ray imaging mission, will be able to take direct X-ray pictures of regions of the size of a black hole event horizon. Both of these space mission will have the ability to give us proofs of black hole existence, and possibly, to distinguish even among different black hole solutions. The project ARISE (Advanced Radio Interferometry between Space and Earth) will use the technique of Space VLBI. The mission, to be launched in 2008, will be based on a 25-meter inflatable space radio telescope working between 8 and 86 GHz [13]. ARISE will provide resolution of 15 $\mu\text{arc-seconds}$ or better, 5-10 times better than that achievable on the ground. At frequencies of 43 and 86 GHz, this would imply resolution of light weeks to light months in distant quasars and will complement the gamma-ray and X-ray observations. ARISE, then, could also study gravitational lenses at resolutions of tens of $\mu\text{arc-seconds}$, and as such, could prove important in the detection of charged black holes. However, it is not only resolution what is needed in order to detect the relativistic images. The main problem will be that they are very much demagnified. They would certainly pose a challenge to observations, if ever possible, enhanced by the fact that the relativistic images are closed to the non-relativistic ones, which are much more intense.

Acknowledgements

We gratefully acknowledge discussions with Salvatore Capozziello and Valerio Bozza (U. of Salerno, Italy). This work has been partially supported by UBA (UBACYT X-143, EFE), CONICET (DFT, and PIP 0430/98, GER), ANPCT (PICT 98 No. 03-04881, GER), and Fundación Antorchas (separate grants to GER and DFT).

Appendix: Deflection angle in terms of elliptic integrals

It is convenient for the calculations to express the integrals of Eqs. (13) and (20) in terms of standard elliptic integrals.

Eq. (13) can be put in the form

$$\alpha(x_0) = \frac{2x_0}{\sqrt{1 - \frac{1}{x_0} + \frac{q^2}{x_0^2}}} \int_{x_0}^{\infty} \frac{dx}{\sqrt{P(x)}} - \pi, \quad (71)$$

where

$$P(x) = x^4 + x_0^2 \left(1 - \frac{1}{x_0} + \frac{q^2}{x_0^2}\right)^{-1} (-x^2 + x - q^2), \quad (72)$$

is a fourth degree polynomial. The four roots of $P(x)$ depend only on x_0 and q and they are real for $x_0 > x_{ps}$ and $|Q| \leq M$. Calling these roots $r_1 > r_2 > r_3 > r_4$, the first one is $r_1 = x_0$ and the others have long expressions (not given here for lack of space) that can be obtained with standard software. Then we can write the exact integral of Eq. (13) as

$$\alpha(x_0) = G(x_0)F(\phi_0, \lambda) - \pi, \quad (73)$$

with

$$G(x_0) = \frac{4x_0}{\sqrt{1 - \frac{1}{x_0} + \frac{q^2}{x_0^2}}} \frac{1}{\sqrt{(r_1 - r_3)(r_2 - r_4)}}, \quad (74)$$

and

$$F(\phi_0, \lambda) = \int_0^{\phi_0} (1 - \lambda \sin^2 \phi)^{-\frac{1}{2}} d\phi, \quad (75)$$

an elliptic integral of the first kind with arguments

$$\phi_0 = \arcsin \sqrt{\frac{(r_2 - r_4)}{(r_1 - r_4)}}, \quad (76)$$

$$\lambda = \frac{(r_1 - r_4)(r_2 - r_3)}{(r_1 - r_3)(r_2 - r_4)}. \quad (77)$$

The derivative of the deflection angle can be expressed:

$$\frac{d\alpha}{dx_0} = F(\phi_0, \lambda) \frac{dG}{dx_0} + G(x_0) \frac{\partial F}{\partial \lambda} \frac{d\lambda}{dx_0} + G(x_0) \frac{\partial F}{\partial \phi_0} \frac{d\phi_0}{dx_0}, \quad (78)$$

and can be written as

$$\begin{aligned} \frac{d\alpha}{dx_0} = & F(\phi_0, \lambda) \frac{dG}{dx_0} + G(x_0) \left(-\frac{E(\phi_0, \lambda)}{2(\lambda - 1)\lambda} - \frac{F(\phi_0, \lambda)}{2\lambda} + \frac{\sin(2\phi_0)}{4(\lambda - 1)\sqrt{1 - \lambda \sin^2 \phi_0}} \right) \frac{d\lambda}{dx_0} + \\ & + \frac{G(x_0)}{\sqrt{1 - \lambda \sin^2 \phi_0}} \frac{d\phi_0}{dx_0}, \end{aligned} \quad (79)$$

where

$$E(\phi_0, \lambda) = \int_0^{\phi_0} (1 - \lambda \sin^2 \phi)^{\frac{1}{2}} d\phi, \quad (80)$$

is an elliptic integral of the second kind with the arguments ϕ_0 and λ given above.

References

- [1] A. Einstein, *Science* **84**, 506 (1936).
- [2] P. Schneider, J. Ehlers, E. E. Falco, *Gravitational Lenses* (Springer Verlag, Berlin, 1992).
- [3] K. S. Virbhadra, G. F. R. Ellis, *Phys. Rev. D* **62**, 084003 (2000). [arXiv:astro-ph/9904193].
- [4] S. Frittelli, T. P. Kling, E. T. Newman, *Phys. Rev. D* **61**, 064021 (2000).
- [5] V. Bozza, S. Capozziello, G. Iovane, G. Scarpetta, *Gen. Rel. Grav.* **33**, 1535 (2001). [arXiv:gr-qc/0102068].
- [6] B. Punsly, *Astrophys. J.* **498**, 640 (1998).
- [7] B. Punsly, G. E. Romero, D. F. Torres, J. A. Combi, *Astron. Astrophys.* **364**, 552 (2000). [arXiv:astro-ph/0007465].
- [8] C. W. Misner, K. S. Thorne, J. A. Wheeler, *Gravitation* (Freeman, New York, 1973).
- [9] S. Weinberg, *Gravitation and Cosmology: Principles and Applications of the General Theory of Relativity* (Wiley, New York, 1972).
- [10] B. Punsly, *Black Hole Gravitohydromagnetics* (Springer Verlag, Heidelberg, 2001).
- [11] Constellation-X web page: <http://constellation.gsfc.nasa.gov/>
- [12] Maxim web page: <http://maxim.gsfc.nasa.gov/>
- [13] Ulvestad J. S., 1999, arXiv:astro-ph/9901374.